Langmuir

Article

pubs.acs.org/Langmuir

Characterization of Silver Nanoparticles in Cell Culture Medium Containing Fetal Bovine Serum

Ulf Hansen and Andreas F. Thünemann*

BAM Federal Institute for Materials Research and Testing, Unter den Eichen 87, 12205 Berlin, Germany

Supporting Information

ABSTRACT: Nanoparticles are being increasingly used in consumer products worldwide, and their toxicological effects are currently being intensely debated. In vitro tests play a significant role in nanoparticle risk assessment, but reliable particle characterization in the cell culture medium with added fetal bovine serum (CCM) used in these tests is not available. As a step toward filling this gap, we report on silver ion release by silver nanoparticles and on changes in the particle radii and in their protein corona when incubated in CCM. Particles of a certified reference material, $\mathbf{p}_1$, and particles of a commercial silver nanoparticle material, $\mathbf{p}_2$, were investigated. The colloidal stability of $\mathbf{p}_1$ is provided by the surfactants polyethylene glycol-25 glyceryl trioleate and polyethylene glycol-20 sorbitan monolaurate, whereas $\mathbf{p}_2$ is stabilized by polyvinylpyrrolidone. Dialyses of $\mathbf{p}_1$ and $\mathbf{p}_2$ reveal that their silver ion release rates in CCM are much larger than in water. Particle characterization was performed with asymmetrical flow field-flow fractionation, small-angle X-ray scattering, dynamic light scattering, and electron microscopy. $\mathbf{p}_1$ and $\mathbf{p}_2$ have similar hydrodynamic radii of 15 and 16 nm, respectively. The silver core radii are 9.2 and 10.2 nm. Gel electrophoresis and subsequent peptide identification reveal that albumin is the main corona component of $\mathbf{p}_1$ and $\mathbf{p}_2$ after incubation in CCM that consists of Dulbecco's modified Eagle medium with 10% fetal bovine serum added.

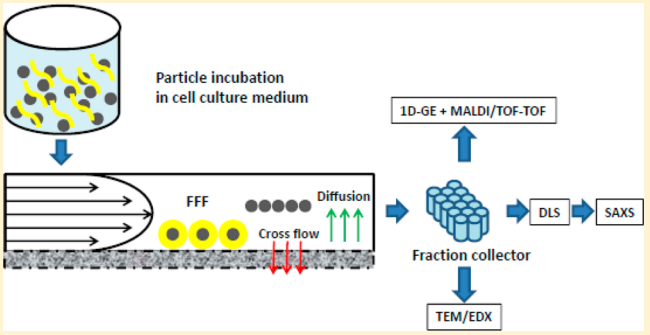

INTRODUCTION

The number of nanoparticle-based consumer products has increased significantly over the past decade. Many products containing silver nanoparticles are used because of the antimicrobial properties of silver.[1] Silver nanoparticles can be found in textiles, refrigerators, cosmetics, dietary supplements, etc.; this makes detailed knowledge of their oral uptake, chemical fate, and toxicity necessary.[2] It has to be noted that a nanomaterial is defined by the European Commission as "a natural, incidental or manufactured material containing particles, in an unbound state or as an aggregate or as an agglomerate and where, for 50% or more of the particles in the number size distribution, one or more external dimensions is in the size range 1 nm−100 nm".[3] Due to the number-weighted basis of this definition, we are convinced that materials easily become nanomaterials when modified with silver nanoparticles. This assumption is based on the fact that a small quantity of particles by weight can produce a tremendous quantity of particles when these particles are counted.

Despite their increasing application, there is an ongoing controversial debate about the toxicologically relevant effects of silver nanoparticles on human health; these effects may depend on diverse particle characteristics, such as radius, morphology, stabilizing agents, and surface charge. These characteristics strongly influence certain properties, such as the adsorption behavior of proteins to the nanoparticles and, hence, the lifetime of these materials in human or animal body fluids.[4] When applied to in vitro models, the administered nanoparticles become dispersed in cell culture medium (CCM), which changes the particle surfaces and associated particle−particle and particle−cell interactions.[5−7] Protein adsorption from the CCM, e.g., Dulbecco's modified Eagle medium (DMEM) with fetal bovine serum added, can cause numerous changes in the physicochemical and toxicological behavior of such nanoparticles, which thus can no longer be related to the untreated particles. Protein adsorption onto the nanoparticle surface normally results in the formation of so-called hard and soft coronas of proteins around the nanoparticles.[8] The structure and composition of these protein coronas depend on the contact time and abundance of available proteins.[7,8] Such a corona alters, for example, the radii of the particles. Typically, the physicochemical characterization of particles in protein-rich media utilizes techniques such as dynamic light scattering (DLS) and transmission electron microscopy (TEM).[5,9,10] However, neither of these techniques alone is sufficient to quantify agglomeration and aggregation, because DLS is very sensitive to a small quantity of aggregates and TEM images often lack statistical significance.

In addition to increasing the total particle radius, proteins substantially change the surface of nanoparticles and, therefore,

Received: February 24, 2015
Revised: May 27, 2015
Published: May 27, 2015

DOI: 10.1021/acs.langmuir.5b00687
Langmuir 2015, 31, 6842−6852

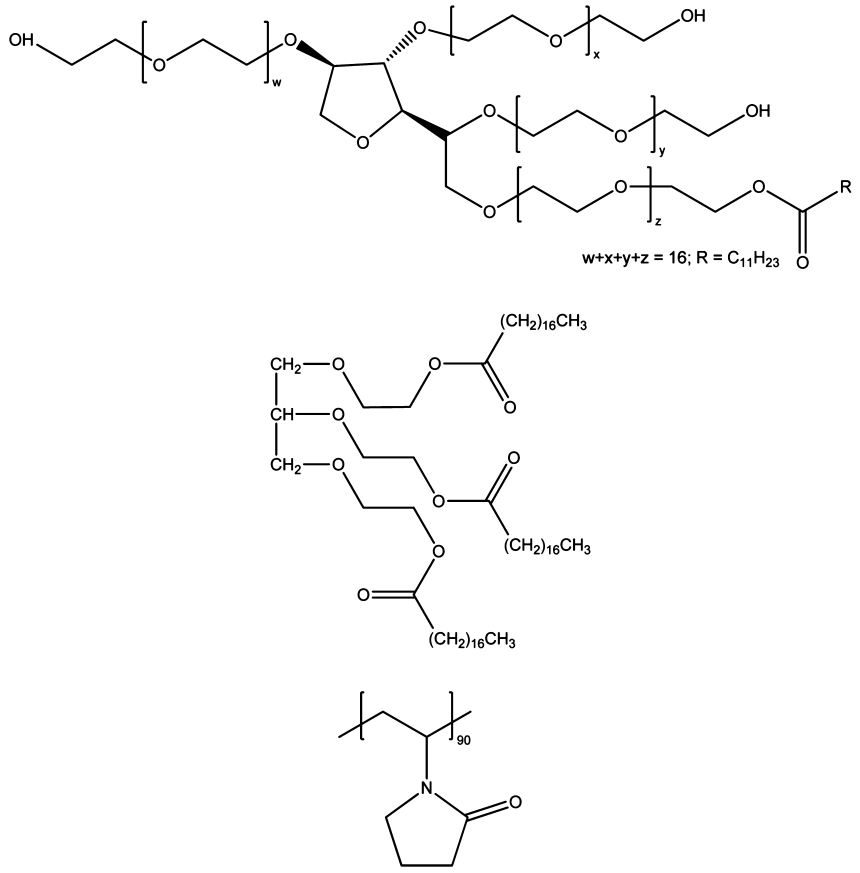

Figure 1. Structures of the molecules that stabilize the silver nanoparticles against aggregation in suspension. $\mathbf{p_1}$ particles are stabilized by a mixture of the nonionic surfactants Tween 20 and Tagat TO V (top and middle structures, respectively). $\mathbf{p_2}$ particles are stabilized by the polymer PVP (lower structure).

alter their interaction with in vitro cell systems. For instance, the adsorption of bovine serum albumin (BSA) to polystyrene nanoparticles altered the uptake of the particles by HeLa cells.[11] Furthermore, a protein corona could alter the uptake and cytotoxicity of nanoparticles dramatically.[12−14] Polystyrene nanoparticles dispersed in the nonionic surfactant polyethylene glycol (PEG)-20 sorbitan monolaurate exhibited a higher affinity to cell membranes than the pristine particles at a surfactant concentration ranging from 0.0025% to 0.05%.[10] That study pointed out that PEG-20 sorbitan monolaurate decreased the cell viability and proliferation rate of Caco-2 cells. Furthermore, Ahamed et al. showed that silver nanoparticles stabilized by polysaccharides are more toxic to different cell types than particles without these biocompatible stabilizers.[15] Stabilizers not only affect the toxicity of the nanoparticles but also the release of silver ions. Many authors claim that the toxicity of silver nanoparticles is related to the induction of oxidative stress, which causes apoptosis in different cell types.[16−18] It is frequently assumed that these effects are based only on the release of silver ions from the nanoparticles. However, there is also evidence for a synergistic impact of nanoparticles and ions.[9,19,20] These studies show that an adequate characterization of the nanoparticles is not only necessary for the raw material but also for nanoparticles subjected to specific experimental conditions. Toxic mechanisms of nanoparticles are influenced by many of their physicochemical properties; the underlying mechanisms are still poorly understood. As a consequence, we believe that it is important to characterize the nanoparticle stock suspension and the particles under relevant experimental conditions in order to be able to make adequate assumptions about the toxicity of nanoparticles from in vitro experiments. Relevant dispersion media are CCMs for in vitro and body fluids for in vivo studies. If knowledge of the particle properties is given only in a pristine state, it is nearly impossible to compare in vitro results from different studies unambiguously. Therefore, such a characterization benefits from techniques that gently separate the nanoparticles from their surrounding medium to minimize protein-corona effects. This separation is ideally followed by a determination of the particle diameters, e.g., DLS, small-angle X-ray scattering (SAXS), and TEM.[21−23] The ion-release properties of the particles could be measured using UV−vis spectroscopy or dialysis.

In this report, silver nanoparticles stabilized with surfactants were chosen for the first type of particles ($\mathbf{p_1}$) and with the biocompatible polymer polyvinylpyrrolidone (PVP) for the second type ($\mathbf{p_2}$). The chemical structures of the stabilizers are shown in Figure 1. $\mathbf{p_1}$ and $\mathbf{p_2}$ have similar hydrodynamic radii, R_h, of 15 and 16 nm but are assumed to display different protein affinities due to their different stabilizers.[24−26] Our recent study suggests that the $\mathbf{p_1}$ particles indeed overcome the gastrointestinal juices in their particulate form and therefore may interact with the intestine when entering the body through oral administration.[22] The particle suspensions were incubated in water and CCM to investigate the influence of the suspending media on the release of silver ions and the changes in their structure, e.g., the appearance of the resulting aggregates. We determined the particles' protein corona in

DOI: 10.1021/acs.langmuir.5b00687
Langmuir 2015, 31, 6842−6852

CCM by means of two-dimensional gel electrophoresis to allow quantification of the expected corona composition.

MATERIALS AND METHODS

Materials. Water used for all preparations was Milli-Q-grade (18.2 MΩ at 25 °C). Cell culture medium used for nanoparticle dispersions was Dulbecco's modified Eagle medium supplemented with 10% fetal bovine serum (FBS) (PAA).

The silver nanoparticles used in this study were $\mathbf{p_1}$ (rent a scientist) coated with PEG-25 glycerol trioleate and PEG-20 sorbitan monolaurate. The original dispersion was diluted from a silver content of 10% (w/w) to a stock dispersion of 2 mg silver mL^{-1} with water. The $\mathbf{p_1}$ particles are available as a certified reference material BAM-N001 (BAM). Additionally, PVP-coated spherical silver nanoparticles $\mathbf{p_2}$ (Nanocomposix) were used as delivered [silver concentration 1 mg mL^{-1} (w/w)].

Sample Preparation for Field-Flow Fractionation (FFF). Silver nanoparticles were either mixed with CCM or water to a final concentration of 500 μg silver mL^{-1} and stored without light in a heating cabinet (Heraeus Function line, Thermo) at 37 °C for 1 day. Subsequently, the nanoparticle suspensions were filtered through a 450 nm poly(ether sulfone) (PES) filter into FFF glass vials and measured after <5 min.

FFF Experiments. FFF data was acquired with an asymmetric flow field-flow fractionation system from Postnova Analytics (Germany). The system consists of an AF2000 focus system, equipped with a PN 5200 auto sampler, PN 7505 inline degasser, PN 1122 tip, and focus pump. Inline solvent filters were placed between the pumps and the channel to reduce background noise. The channel thickness was 500 μm, and the membrane consists of PES with a molecular weight cutoff (MWCO) of 3500 Da. The solvent used was water, containing 0.01% (w/v) sodium dodecyl sulfate (SDS) and 0.2% sodium azide as electrolytes. The flow rates were controlled via AF2000 software (Postnova). A slot-outlet function was implemented by using a modified channel cover with an additional 13 mm port in front of the laminar outlet port and by connecting a narrow capillary to the slot outlet port of the FFF unit to achieve 80% slot flow as a result of backpressure.[27] The slot-outlet was applied to minimize dilution of the particles. A UV detector (Milton Roy; detection at wavelength of 430) was coupled directly to the channel outlet. The fractionation and measurements were performed at 20 ± 1 °C. A fraction collector (Gilson) was additionally connected. A sample of 100 μL with a silver content of 500 μg mL^{-1} was injected. We used an injection time of 6 min and an injection flow of 0.1 mL min^{-1} with a cross-flow of 1.5 mL min^{-1} and then an exponential cross-flow decay over 40 min to a flow of 0 mL min^{-1}. The fractionation was started 1 min after the silver peak occurred in the UV detector signal due to eluent run time through the capillaries, and the procedure was repeated two times to yield a sufficient volume of sample material.

Centrifugation. particle $\mathbf{p_1}$ was dispersed in CCM at a concentration of 25 μg silver mL^{-1} and stored at 37 °C for 1 day without light in a heating cabinet (Heraeus Function line, Thermo). Subsequently, the dispersions were centrifuged three times with a Heraeus 3SR+ (Thermo) at 10 000g for 20 min. Following the first and second centrifugation, the supernatant was discarded, and the precipitate was suspended with PBS. After the third centrifugation, 30 μL of reducing SDS sample buffer (Sigma) was used as the dispersion medium, and the resulting fluid was heated to 95 °C for 5 min. After centrifugation at 10 000g for 5 min, the supernatant was transferred to a one-dimensional electrophoresis (1-DE) gel.

DLS Measurements. The DLS measurements were performed using a Malvern Instruments particle sizer (Zetasizer Nano ZS, Malvern Instruments, UK) equipped with a He−Ne laser (λ = 632.8 nm). The scattering data were recorded at 25 ± 1 °C in backscattering modus at a scattering angle of 2θ = 173°, which corresponded to a scattering vector of $q = 4\pi n/\lambda \sin\theta$ (0.02638 nm^{-1}). Samples used for analysis were fractions A−D from the FFF separation without further preparation.

SAXS Measurements. SAXS measurements were performed in a quartz capillary with an SAXSess Kratky-type instrument (Anton Paar) at 25 ± 1 °C. The SAXSess has a low sample-to-detector distance (0.309 m), which is appropriate for investigation of dispersions with low scattering intensities. The measured intensity was corrected by subtracting the intensity of a capillary filled with pure water. The scattering vector is defined in terms of the scattering angle (θ) and the wavelength (λ) of the radiation (λ = 0.154 nm); thus, $q = 4\pi/\lambda \sin\theta$. Deconvolution (slit length desmearing) of the SAXS curves was performed with Glatter's established indirect Fourier transformation method implemented in the PCG Software Version 2.02.05 (University of Graz) to verify the results produced with the SAXS-Quant software. Samples analyzed with SAXS were prepared similarly to those for FFF separation experiments. Curve fitting was performed with SASfit software (Paul Scherrer Institute) and curve simulation by Monte Carlo methods with the McSAS software.[28,29]

Two-Dimensional Electrophoresis (2-DE) Gels. Nanoparticles used for 2-DE gels were fractions B and D from the FFF separation. The suspensions were centrifuged three times at 2500g for 15 min. After the first and second centrifugation steps, the supernatant was discarded, and the remaining pellet was resuspended in PBS. Subsequent to the third centrifugation step, the pellet was resuspended in 100 μL of lysis-buffer containing 7 M urea (Serva), 2 M thiourea (Serva), 0.16% (m/v) Serdolit (Serva), 4% (m/v) 3-[(3-cholamidopropyl)dimethylammonio]-1-propanesulfonate (CHAPS) (BioRad), 2% (v/v) Pharmalyte (GE Healthcare), 1.5% (v/v) DeStreak reagent (GE Healthvare), 0.6% (w/v) spermine (Sigma), and water (proteome grade, BioRad). Additionally, 350 μL of rehydration-buffer containing 42% (w/v) urea, 17% (w/v) thiourea, 1.5% (v/v) CHAPS, 1.2% (v/v) DeStreak reagent, 0.5% IPG buffer (pH 3−10, GE Healthcare), and water was added. The solution was transferred to Immobiline DryStrip Gels (GE Healthcare), and isoelectrical focusing was performed with an Ettan IPGphor 3 (GE Healthcare) for 40 h. Focused 1-DE gels were loaded on 10% acrylamide gels and the 2-D separation was performed with an Ettan Dalt XII separation unit (GE Healthcare). Completed gels were stored at 4 °C until further preparation for MALDI-analysis.

MALDI-Tof/Tof Measurements. The protein bands from the 1-DE and 2-DE gels were excised, and after washing, reduction with DTT (Merck), and carbamidomethylization with iodoacetamide (Merck), they were in-gel digested with trypsin (Roche). The resulting peptide mixtures were analyzed with an Ultraflex II TOF/TOF (Bruker) and the implemented Biotools 3.2 software. Peptide identification was conducted with Mascot (Matrix Science) software.

TEM Imaging. One drop of the FFF fractions was dried, on a dust-free carbon-coated copper-grid and TEM images were taken with an analytical TEM (JEM 2200FS, JEOL) at 200 kV.

Inductively Coupled Plasma Mass Spectrometry (ICP-MS) Analysis. One- and 7-day dialyses were conducted of 3 mL of a 25 μg silver mL^{-1} NP suspension for both nanoparticles in (a) FBS, (b) 6.4 g L^{-1} NaCl (Merck) solution, and (c) water in the dark using a cellulose ester dialysis membrane (Spectra/Por, Spectrum Laboratories) with a cut off from 500−1000 Da with 500 mL of water at 37 °C under constant agitation. The initial pH values were 7.5, and the final values were 7.0 in CCM. The corresponding values in water were 6.5 and 6.3, respectively. The dialysis reservoirs were enclosed 500 mL glass flasks and were opened only briefly for sampling. After 1 and 7 days, respectively, the dialysis membrane was removed and 50 mL of ultrapure 34% HCl (Carl Roth) was added; the solution was stirred for 10 min. Then, 5 mL of the reservoir outside the membrane was mixed with 5 mL of ultrapure 70% HNO_3 (Carl Roth, Germany) and analyzed with ICP-MS (X-series II, Thermo).

Cell Line and Viability and Toxicity Assays. The human colon adenocarcinoma cell line Caco-2 was obtained from the European Collection of Cell Cultures (ECACC, Porton Down). Cells were kept in DMEM (PAN Biotech) at 37 °C in a humidified atmosphere of 5% CO_2. All media were supplemented with 10% (v/v) FBS and 1% (v/v) penicillin/streptomycin. Caco-2 cells were cultured in tissue culture flasks for propagation (75 cm^2) and in 96-well plates for experiments. After exposure of the cells, cell viability and the proliferation of Caco-2

DOI: 10.1021/acs.langmuir.5b00687
Langmuir 2015, 31, 6842−6852

cells were assessed utilizing the commonly used Promegas CellTiter Blue (CTB) assay. The CTB assay is based on the ability of living cells to convert resazurin into resorufin and measures the oxidative metabolism. Nonviable cells rapidly lose their metabolic capacity and thus do not generate a fluorescent signal. For the CTB assay, the Caco-2 cells were plated into 96-well plates at a density of 10×10^3 cells per well in culture medium. Cells were allowed to attach for 1 day before treatment. Subsequently, the culture medium was replaced with 100 μL of medium control and different concentrations of silver nanoparticles. Cells were exposed for 1 day. Finally, CTB reagent was added to each well, and the resulting solution mixture was incubated for an additional 2 h and measured on a microplate reader with 540 nm excitation and 590 nm emissions. The medium control was set to 100%. Means and standard deviations were calculated from at least three independent experiments.

RESULTS AND DISCUSSION

Silver Ion Release. The impact of silver ions on the toxicity of silver nanoparticles is discussed ambivalently in the literature. However, all authors agree that silver nanoparticles are a steady source of silver ions to the surrounding media. Therefore, we first investigated the silver ion release from $\mathbf{p_1}$ and $\mathbf{p_2}$ dispersed in water and in CCM to determine whether differences in stabilizer, medium, and concentration have a significant influence. Dialyses of dispersions with a total initial silver concentration of 2.5 and 25.0 μg mL^{-1} were performed for this purpose at a temperature of 37 °C for 1 and 7 days. The setup is shown in Figure 2. The silver ion content in ultrapure water as dialysis medium was determined by ICP-MS. The ratio of the volume of the dialysis tube to the volume of the dialysate reservoir was 1 to 100. The results for the quantities of released silver in terms of mass release and in percentage of the available silver are summarized in Table 1. Values for released silver in percentage of the initial quantity of silver are additionally given in Figure 3. It can be seen that the quantity of released silver ions is generally much larger in CCM than in water. The largest effect is observed for $\mathbf{p_1}$ at a concentration of 2.5 μg mL, where no silver release was detected in water, but complete release was seen in CCM. A smaller percentage of silver ions was released at the higher initial concentration of 25.0 μg mL than at the lower concentration of 2.5 μg mL. Furthermore, the differences between CCM and water are more pronounced for $\mathbf{p_1}$ than for $\mathbf{p_2}$, but the differences between dialysis times of 1 and 7 days are small. Obviously, the equilibrium between the silver ion containing dialysate and silver ion resource became established within 24 h. Note that, if the dialysate had been changed during dialysis, the release of silver ions obviously could have proceeded.[30] However, we did not change the dialysate in our study because this would not be comparable to cell culture experiments, in which the nanoparticle dispersion under study usually is not changed during the exposure time.

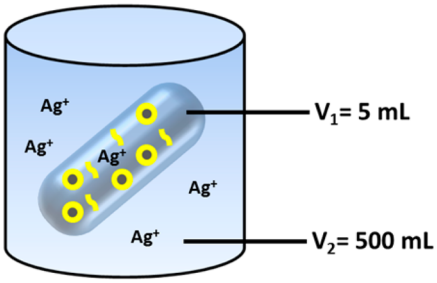

Figure 2. Dialysis setup for monitoring the release of silver ions from silver nanoparticles. The volume of the dialysis tube was 5 mL and the volume of the dialysis reservoir was 500 mL.

It is surprising that the CCM results in the release of a much higher quantity of silver ions. A possible explanation for the more rapid dissolution of the particles in CCM compared to water could be the formation of soluble $AgCl_2^-$ and $AgCl_3^{2-}$ at high Cl^- concentrations, which is 120 mM in the CCM.[31] The formation of AgCl in the dialysis medium can be excluded because of the rapid transport of Cl^- and Ag^+ to the bulk water. Contingently, existing silver chloride species in the bulk water were dissolved by adding concentrated hydrochloric acid prior to ICP-MS measurements. Another possible explanation for the high silver ion release in CCM could be nteractions of the dissolved ions with free cysteine and cysteine groups of proteins in CCM. These amino acids are known to remove free silver ions from solution and thereby shift the equilibrium toward the release of more silver ions.[32] The particles show an equilibrium between dissolved and particulate silver after at least 4 days in CCM. In water, $\mathbf{p_1}$ reached equilibrium shortly after dispersion, whereas $\mathbf{p_2}$ exhibited an increasing Ag^+ release. Slower dissolution rates for $\mathbf{p_1}$ in water may be due to the high stabilizer concentration, which provides a brushlike structure of PEO chains on the particles' surface. These chains bind water molecules relatively tightly via hydrogen bonds and form a water shell outside the brush, which reduces the contact of free oxidizing species with the silver surface.[33,34] In any case, it is obvious that the different stabilizers influence the quantity of released silver ions in water and in CCM differently.

The dissolution of silver ions is a complex phenomenon and cannot be understood by applying a simple model, but we measured the silver ion release curves from the CCM to the water reservoir, as shown in Figure 4. The curve shapes are similar to those observed for the release of silver ions from pure

Table 1. Release of Silver Ions from $\mathbf{p_1}$ and $\mathbf{p_2}$ Silver Nanoparticles Measured with ICP-MS after Dialysis in Water and CCM[a]

	μg of Ag^+			
	$\mathbf{p_1}$		$\mathbf{p_2}$	
incubation time (days)	H_2O	CCM	H_2O	CCM
	Initial Quantity of Silver: 12.5 μg (c = 2.5 μg mL^{-1})			
1	–[a]	11.2 ± 1.5 (89.6 ± 12%)	2.8 ± 0.4 (22.4 ± 3.2%)	8.3 ± 1.1 (66.4 ± 8.8%)
7	–[a]	11.6 ± 1.5 (92.8 ± 12%)	3.6 ± 0.5 (28.8 ± 3.7%)	10.7 ± 1.4 (85.6 ± 11.2%)
	Initial Quantity of Silver: 125.0 μg (c = 25.0 μg mL^{-1})			
1	7.0 ± 1.4 (5.6 ± 1.1%)	47.0 ± 6.1 (37.6 ± 4.9%)	9 ± 1.2 (7.2 ± 1%)	77.0 ± 10.0 (61.6 ± 8.0%)
7	7.3 ± 1.5 (5.7 ± 1.1%)	57.0 ± 7.4 (45.6 ± 5.9%)	30.6 ± 3.9 (24.5 ± 3.2%)	72.0 ± 9.4 (57.6 ± 7.7%)

[a]The concentration was below the limit of detection. [a]The temperature during dialysis was 37 °C. Times of dialysis were 1 and 7 days. The total amount of silver in the dispersions prior to dialysis was 12.5 and 125 μg in 5 mL, corresponding to initial concentrations of 2.5 and 25 μg mL^{-1}.

DOI: 10.1021/acs.langmuir.5b00687
Langmuir 2015, 31, 6842–6852

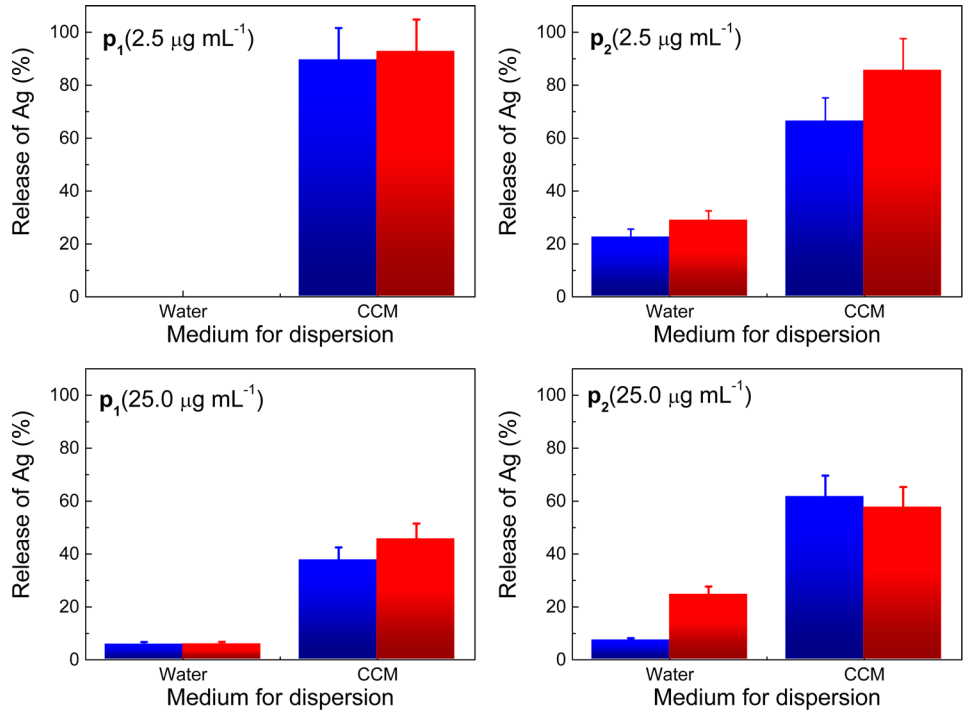

Figure 3. Release of silver ions from particles $\mathbf{p_1}$ and $\mathbf{p_2}$ measured with ICP-MS after dialysis times of 1 and 7 days (blue and red bars, respectively). The initial concentrations of total silver content were 2.5 and 25.0 μg mL^{-1}, respectively.

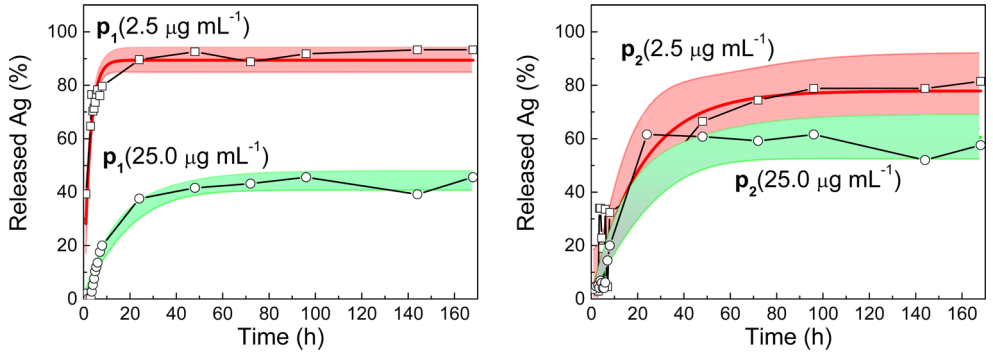

Figure 4. Release kinetics of silver ions from $\mathbf{p_1}$ and $\mathbf{p_2}$ in CCM dialyzed against Milli-Q water at 37 °C for 1 week. The dialysis membrane consisted of cellulose ester with a molar weight cutoff at 500−1000 g mol^{-1}. Initial silver concentrations of the nanoparticle suspensions were 2.5 μg mL^{-1} (squares) and 25.0 μg mL^{-1} (circles). Analysis of the released silver ion was conducted using ICP-MS. The results of fitting a modified first order reaction are given (solid lines), including their confidence intervals at a 95% level (transparent areas).

water as reported by Kittler et al.[35] In analogy to their study, we also utilized a modified first-order reaction kinetic rate equation of the form

$$y(t) = y_{\text{final}}[1 - \exp(-kt)] \quad (1)$$

for data description. The $y(t)$ is the released quantity of silver ions as a percentage of the initial value, y_{final} is the extrapolated value of released silver ions for infinite times, k is a formal rate constant, and t is the experimental time in hours. The optimal values for y_{final} and k were determined from the curve fits, as shown in Figure 4 (solid lines). The 95% confidence intervals are shown in the figure (shaded areas). Best fit values for y_{final} of $\mathbf{p_1}$ are 89 ± 2% and 44 ± 2% at concentrations of 2.5 and 25.0 μg mL^{-1}. The corresponding values for $\mathbf{p_2}$ are 78 ± 7% and 61 ± 4%. These values are close to the values given in Figure 3, as must be expected if the silver ion release has reached completion at the end of the experimental time of 1 week. The k-values can be utilized for easier interpretation to calculate the time τ required to release 50% of silver ions contained in y_{final} using

$$\tau = \ln(2) \times k^{-1} \quad (2)$$

The τ-values are 1.8 ± 0.3 and 12 ± 2 h for $\mathbf{p_1}$ at concentrations of 2.5 and 25.0 μg mL^{-1}, respectively. The corresponding values for $\mathbf{p_2}$ are 15 ± 6 and 14 ± 3 h. All values are summarized in Table 2. It is obvious that the release kinetics of $\mathbf{p_1}$ at the low concentration of 2.5 μg mL^{-1} is approximately 7 times faster than at the higher concentration of 25.0 μg mL^{-1}. In contrast, no significant difference in τ is observed for $\mathbf{p_2}$ at these two concentrations. The lower uncertainty values for τ of 0.3 and 2 h for $\mathbf{p_1}$ compared to 6 and 3 h for $\mathbf{p_2}$ indicate that the release of silver ions is more structured in the case of $\mathbf{p_1}$ than $\mathbf{p_2}$. The lower uncertainties result in smaller confidence intervals, which are displayed in Figure 4.

Cell Viability. A concentration-dependent effect on cell viability is to be expected for both silver nanoparticles.

DOI: 10.1021/acs.langmuir.5b00687
Langmuir 2015, 31, 6842−6852

Table 2. Fit Parameters for the Release of Silver Ions, Calculated for Formal First-Order Kinetics According to Eq 1[a]

particles	concn (μg mL^{-1})	y_{final} (%)	k (h^{-1})	τ (h)
$\mathbf{p_1}$	2.5	89 ± 2	0.300 ± 0.060	1.8 ± 0.3
$\mathbf{p_1}$	25.0	44 ± 2	0.058 ± 0.007	12 ± 2
$\mathbf{p_2}$	2.5	78 ± 7	0.047 ± 0.020	15 ± 6
$\mathbf{p_2}$	25.0	61 ± 4	0.048 ± 0.010	14 ± 3

[a]The temperature during dialysis was 37 °C. Dialysis times were 1 and 7 days. The total quantity of silver in the dispersions prior to dialysis was 12.5 and 125 μg in 5 mL, corresponding to initial concentrations of 2.5 and 25 μg mL^{-1}.

Therefore, we employed an in vitro cytotoxicity assay on Caco-2 cells to quantify the expected effect. Indeed, the cell viability decreases with increasing concentration of $\mathbf{p_1}$ and $\mathbf{p_2}$, as shown in Figure 5. Tentatively, we used a linear model to interpret the cell viability; this resulted in a decrease of 0.59 ± 0.08% per μg mL^{-1} for $\mathbf{p_1}$ and 0.60 ± 0.03% per μg mL^{-1} for $\mathbf{p_2}$. We can therefore conclude that no differences between $\mathbf{p_1}$ and $\mathbf{p_2}$ can be detected within the experimental uncertainty limits with respect to the reduction of cell viability. At first glance, this result seems contradictory, because the silver ion release from $\mathbf{p_1}$ at a low concentration of 2.5 μg mL^{-1} is much faster than for $\mathbf{p_2}$. But it can be seen in Figure 5 that no significant effect of the particles on the cell viability can be detected at concentrations below 20 μg mL^{-1}. In conclusion, the differences in silver release kinetics at concentrations lower than a threshold of 20 μg mL^{-1} are not relevant for the viability of Caco-2 cells. We also measured the viability of the cells in the presence of silver in the form of silver nitrate and in the presence of the stabilizers. We found that the stabilizers have no measurable impact on the viability at concentrations of up to 100 μg mL^{-1}, as shown in the bar diagram in Figure 5. This result was expected, but the silver in form of silver nitrate produces a decrease of 4.0 ± 0.6% per μg mL^{-1}, which is a factor of 6 to 7 times larger than that produced by the particles. In addition, the cell viability is slightly, but significantly, reduced by about 10% at low silver salt concentrations in a range of 2−3%. In this concentration range, the nanoparticles have no effect on cell viability, although they release most of the silver in the form of ions. In all probability, the silver ions from the nanoparticles are masked by proteins, and this suppresses cell viability effects below a certain threshold value.

Separation of Particles from CCM. In any case, we must expect that the cell culture medium interacts substantially with the nanoparticles. In order to shed light on this interaction, we performed a detailed characterization of the $\mathbf{p_1}$ and $\mathbf{p_2}$ particles after incubation in water and CCM at 37 °C for 1 day. We used these conditions because the data given above showed that an equilibrium state is generally achieved after 1 day, and in addition, similar conditions have been used for previous cytotoxicity tests.[36] After incubation, we were interested in revealing whether the CCM produces changes of structure of the particles in comparison to water. The nanoparticles must be separated from the excess protein for this purpose. In this case, we utilized FFF because of the low shear forces it exerts during nanoparticle separation. Other methods, e.g., ultracentrifugation and size exclusion chromatography, produce much higher shear forces that may ablate proteins from the nanoparticle surface.[37] We performed UV detection during FFF fractionation at wavelengths of 430 and 280 nm, which are the absorption maxima of the nanoparticles as well as the amino acids tryptophan and tyrosine, respectively.[38] These amino acids are components of the proteins present in our CCM. The UV absorption of the nanoparticles dispersed in water and CCM, respectively, are shown in Figure 6 as a function of the fractionation time. It can be seen that the particles dispersed in CCM eluted later than the particles dispersed in water. In water, $\mathbf{p_1}$ eluted at fractionation times between 15 and 30 min with a maximum at 17 min. In CCM, $\mathbf{p_1}$ eluted between 18 and 38 min with a maximum at 22 min. Similarly, $\mathbf{p_2}$ in water eluted between 15 and 22 min with a maximum at 17 min. In CCM, the $\mathbf{p_2}$ eluted between 19 and 40 min with a maximum at 23 min. The maximum in the trace of the two particles in CCM is shifted to later times by approximately 5−6 min. Additionally, the width of the peak increases from 15 to 20 min for $\mathbf{p_1}$ and from 7 to 21 min for $\mathbf{p_2}$. Obviously, the shift of the maxima

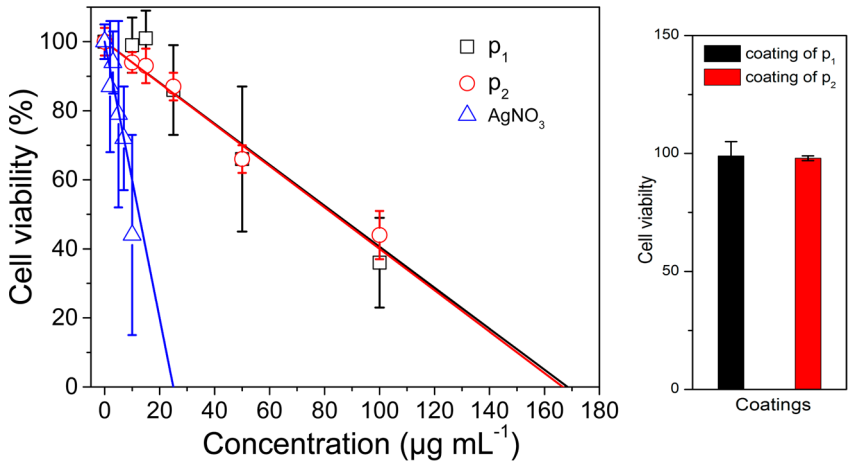

Figure 5. Cell viability of Caco-2 cells as a function of the concentration of particles $\mathbf{p_1}$ and $\mathbf{p_2}$ (left-hand panel). For comparison, the stabilizing surfactants of $\mathbf{p_1}$ and the stabilizing PVP of $\mathbf{p_2}$ alone induced no change of cell viability at a concentration of 100 μg mL^{-1}, which is the value of the highest nanoparticle concentration (right-hand panel). The Caco-2 cells were seeded in 96-well plates at a density of 10^4 cells per well and cultured for 1 day before treatment. Cells were then incubated with medium control and different concentrations of $\mathbf{p_1}$ and $\mathbf{p_2}$. Cell viability was measured using the Promegas CellTiter Blue (CTB) assay. The medium control was set to 100%. The experiment was repeated three times and the standard deviation was calculated. Significant cellular toxicity was apparent at 50 μg Ag mL^{-1} for both particles.

DOI: 10.1021/acs.langmuir.5b00687
Langmuir 2015, 31, 6842−6852

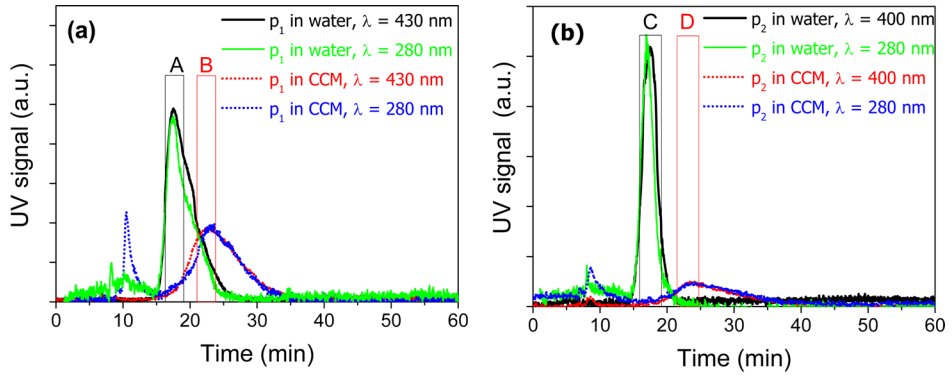

Figure 6. FFF elugrams of suspensions of $\mathbf{p_1}$ and $\mathbf{p_2}$ silver nanoparticles in water and CCM (solid and dotted curves, respectively). The UV signals are displayed as a function of fractionation time at the particles' absorption maximum of 430 nm for $\mathbf{p_1}$ (a) and 400 nm for $\mathbf{p_2}$ (b). In addition, the signals measured at 280 nm are shown for both. The total silver concentrations were 500 μg mL^{-1}. All suspensions were incubated in the dark at 37 °C for 1 day. The fractions around the peak maxima, marked with rectangles in the figures, were used for DLS and TEM measurements. Samples were collected at elution times between 16 and 18 min (fraction A), 21 and 23 min (fraction B), 16 and 18 min (fraction C), and 23 and 25 min (fraction D). Curve maxima of the particles in CCM are shifted toward later retention times of 5 min for $\mathbf{p_1}$ and 7 min for $\mathbf{p_2}$ in comparison to the particles in water. These shifts indicate increased R_H due to a protein corona.

correspond to higher hydrodynamic radii of the particles in CCM than in water.[39] This width increase can be interpreted as an increase in the width of the particles' radii distributions. These radii increases and radii distribution broadenings are either a result of particle aggregation or particle growth, e.g. caused by protein adsorption.

Core Radii Distribution. Next, SAXS measurements were performed in order to reveal whether particle aggregation or protein adsorption causes the observed differences in the FFF retention times. We expected that SAXS would be highly sensitive to particle aggregation but hardly sensitive at all to the formation of a protein corona. Since the SAXS intensity is proportional to the square of the density difference between nanoparticle and its surroundings, the contrast of a silver nanoparticle in water is about 750 times higher than that of a protein. The measured SAXS data were initially fitted using a spherical model of the silver cores and Gaussian radii distribution. Differential volume-weighted distributions of $\mathbf{p_1}$ and $\mathbf{p_2}$ in water are shown in the top row of Figure 7 (parts a and b, respectively). The corresponding curves of the particles in CCM are displayed in the middle row (Figure 7, parts c and d, respectively). The insets display the corresponding SAXS data and fit curves (gray and blue curves, respectively). Curve fits for $\mathbf{p_1}$ reveal particle radii of R = 6.5 ± 0.1 nm before (Figure 7a) and 6.9 ± 0.1 nm after incubation in CCM (Figure 7c). The values of $\mathbf{p_2}$ are R = 9.6 ± 0.1 nm (Figure 7b) and 9.7 ± 0.1 nm (Figure 7d), respectively. The widths of the radii distributions are 1.3 nm for $\mathbf{p_1}$ and 1.5 nm for $\mathbf{p_2}$, and they are the same for water and CCM. It is obvious from inspection of the curve fits that the resulting Gaussian radii distributions must considered as a rough estimate.

Therefore, we applied a recently developed Monte Carlo approach, which allows form-free simulations of the SAXS data.[28] The resulting curves simulate the measured SAXS curves within their experimental error (black and red solid curves of the insets), and the volume-weighted radii distributions are presented as histograms. The Monte Carlo simulation derived mean radii are R = 9.2 ± 0.1 nm for $\mathbf{p_1}$ in water and 9.5 ± 0.1 nm in CCM. The corresponding values for $\mathbf{p_2}$ are R = 10.2 ± 0.1 and 11.2 ± 0.2 nm. The width of the radii distributions are 3.4 and 3.1 nm for $\mathbf{p_1}$ in water and CCM, respectively. For $\mathbf{p_2}$ the widths are 2.2 and 4.6 nm. Obviously, the increased width of $\mathbf{p_2}$ is caused by a small, but significant, quantity of aggregates. This difference is more obvious in the cumulative presentation of the radii distributions in Figure 7e,f, in which no aggregation is detectable for $\mathbf{p_1}$ and approximately 5% aggregation is seen for $\mathbf{p_2}$ in CCM, with radii of the aggregates between 25 and 33 nm. To conclude the discussion of the SAXS analysis, it was found that $\mathbf{p_1}$ displays an asymmetric core radii distribution, which does not change in CCM. In contrast, $\mathbf{p_2}$ displays a symmetric core radii distribution, which is prone to a small but significant core aggregation in CCM. Therefore, aggregation is not the reason for the longer FFF retention times of the particles in CCM compared to water.

Particle Corona. This finding leads to the assumption that instead of aggregation, the formation of a large protein corona around the particles after their incubation in CCM is very probable. In order to prove this assumption, DLS measurements were performed. They provide the hydrodynamic radius and are therefore a measure of radii of the whole particles, i.e., core plus corona. The DLS results for $\mathbf{p_1}$ and $\mathbf{p_2}$ after FFF separation are shown in Figure 8 (left- and right-hand panel, respectively). Given are intensity-weighted radii distributions in differential and cumulative presentation of the particles in water (black solid curves) and in CCM (red dotted curves). The peak maxima are at R_h = 15 ± 1 and 23 ± 3 nm for $\mathbf{p_1}$ in water and CCM, respectively. The corresponding widths of the radii distributions for $\mathbf{p_1}$ are 5 and 14 nm, respectively. The maxima of $\mathbf{p_2}$ are R_h = 16 ± 1 and 39 ± 5 nm. The widths of the radii distributions for $\mathbf{p_2}$ are 8 and 29 nm, respectively. The difference between hydrodynamic radius and core radius, $\Delta R_{stabilizer} = R_h - R$, is an estimate of the thickness of the layer formed by the stabilizer. This layer is about 4−5 nm for $\mathbf{p_1}$ and $\mathbf{p_2}$. Additionally, we can estimate the thickness of the protein corona from the differences in the particles' R_h values, $\Delta R_{protein} = R_{h,CCM} - R_{h,water}$. This assumption seems reasonable, since no or little aggregation of the cores was detected for $\mathbf{p_1}$ or $\mathbf{p_2}$, respectively. Under these assumptions, the protein layer thicknesses are approximately 8 ± 3 and 23 ± 5 nm for $\mathbf{p_1}$ and $\mathbf{p_2}$. The protein layer appears to be thinner and more defined for $\mathbf{p_1}$ than for $\mathbf{p_2}$. The main protein component of the CCM is bovine serum albumin, which amounts to 85 wt %. It has dimensions of 8.4 × 8.4 × 3.15 nm.[40] When taking these

DOI: 10.1021/acs.langmuir.5b00687
Langmuir 2015, 31, 6842−6852

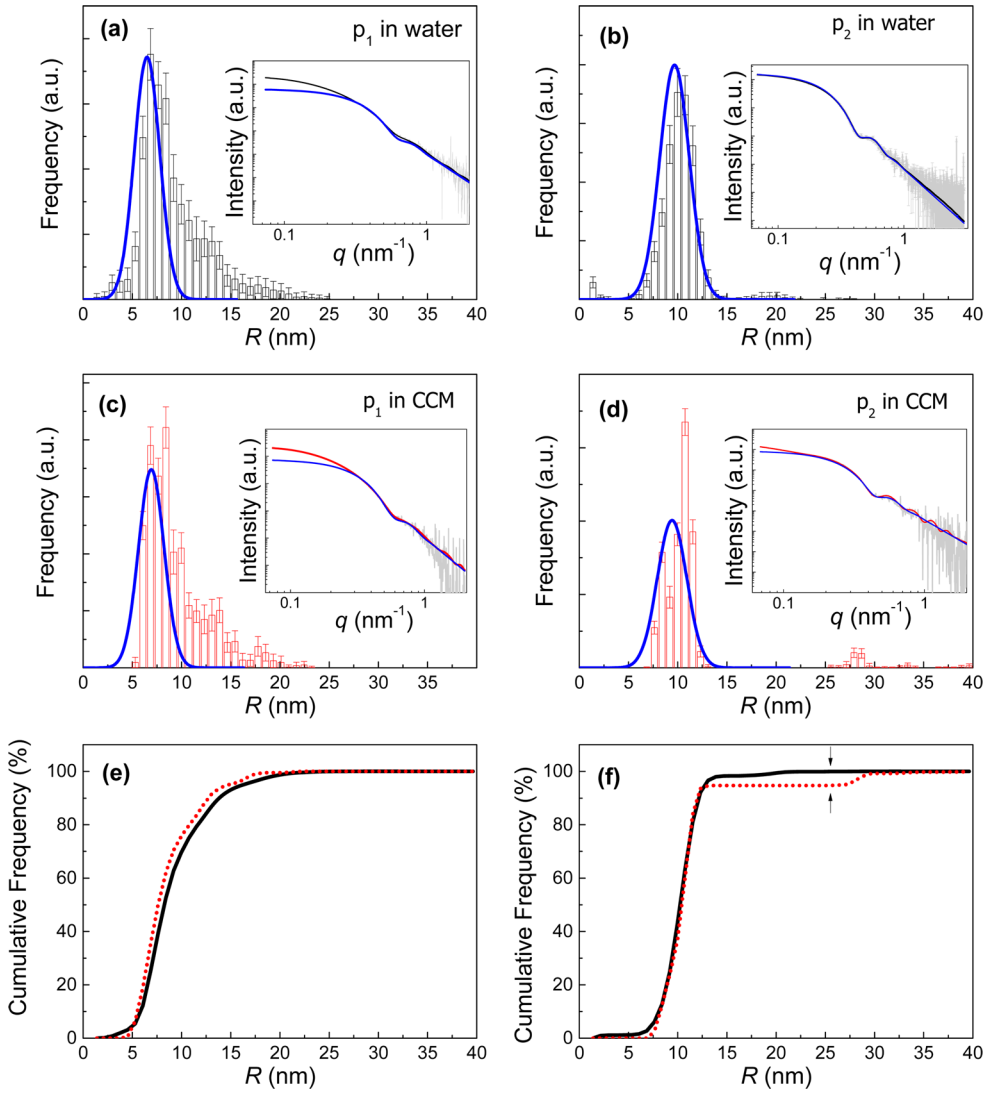

Figure 7. Radii distributions of the silver cores of the particles as determined with SAXS. Differential volume-weighted distributions of $\mathbf{p_1}$ and $\mathbf{p_2}$ in water are shown in the top row (a and b, respectively). The corresponding curves of the particles in CCM are displayed in the middle row (c and d, respectively). Gaussian radii distributions are derived from curve fits (blue curves), whereas the histograms are derived from form-free simulations of the SAXS data.[28] The insets display the corresponding SAXS data, fit curves, and simulation curves. Curve fits for $\mathbf{p_1}$ reveal particle radii of $R = 6.5 \pm 0.1$ nm before (a) and 6.9 ± 0.1 nm after (c) incubation in CCM. The values of $\mathbf{p_2}$ are $R = 9.6 \pm 0.1$ nm (b) and 9.7 ± 0.1 nm (d), respectively. The widths of the radii distributions are 1.3 nm for $\mathbf{p_1}$ and 1.5 nm for $\mathbf{p_2}$, and they are the same for water and CCM. The simulations using the Monte Carlo approach reproduce the measured curves significantly better (black and red solid curves of the insets). The Monte Carlo simulation derived mean radii for $\mathbf{p_1}$ in water and CCM are $R = 9.2 \pm 0.1$ and 9.5 ± 0.1 nm, respectively. The values for $\mathbf{p_2}$ are $R = 10.2 \pm 0.1$ and 11.2 ± 0.2 nm. The width of the radii distributions are 3.4 and 3.1 nm for $\mathbf{p_1}$ in water and CCM, respectively. The corresponding widths of $\mathbf{p_2}$ are 2.2 and 4.6 nm. The cumulative presentation of the radii distributions in parts e and f display no aggregates for $\mathbf{p_1}$ and about 5% aggregates for $\mathbf{p_2}$ in CCM, with radii between 25 and 33 nm.

dimensions and the fact that a volume-equivalent sphere has a radius of 6 nm into account, we assume that a protein monolayer forms the protein corona of $\mathbf{p_1}$. In contrast, a diffuse multilayer of approximately three to four protein layers on average can be assumed for $\mathbf{p_2}$.

In order to verify our findings from SAXS and DLS, we analyzed the FFF fractions with STEM/TEM in combination with energy dispersive X-ray spectroscopy. The STEM/TEM pictures as displayed in Figure S1 (Supporting Information) prove that the particles are spherical with radii ranging from ca. 20 to 25 nm. The gray shades around the particles may originate from surrounding medium residues after particle preparation for TEM. The pictures from STEM with EDX in Figures S1c and S2b (Supporting Information) show an accumulation of sulfur in the periphery of the particles after incubation in CCM. We assume that the sulfur results from adsorption of proteins to the particles. Binding of proteins to the particles' surfaces seems unlikely, since they are densely covered with the stabilizer. If that is the case, the interaction is dominated by van der Waals forces and Coulomb interactions. A coordinative binding of proteins to the silver nanoparticle surface can occur, e.g., via the thiol groups of cysteine and carboxyl groups of the amino acids.[41,42] BSA, as the most abundant protein in FBS, has about 30 cysteine groups. However, without any conformational changes of the protein, there is only one cysteine group available (Cys-34) for a covalent binding to the silver core.[7] Nonetheless, BSA and other proteins undergo changes in their secondary structure

DOI: 10.1021/acs.langmuir.5b00687
Langmuir 2015, 31, 6842−6852

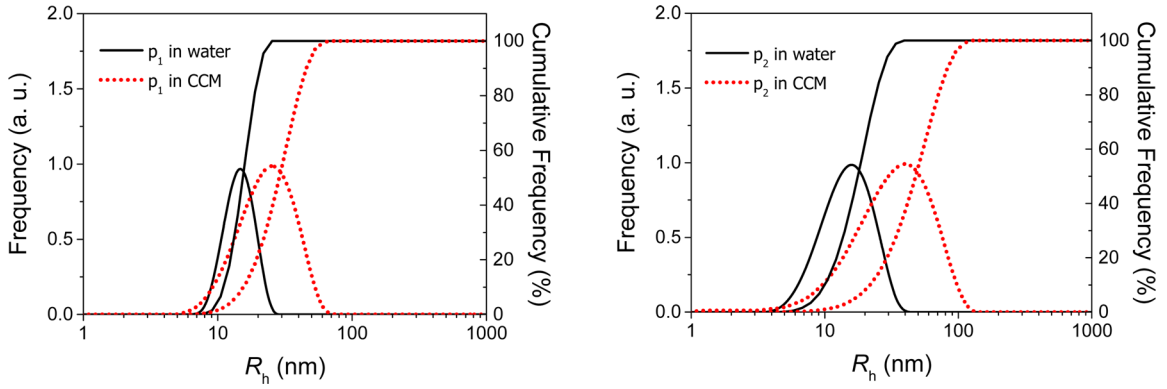

Figure 8. DLS results for $\mathbf{p_1}$ and $\mathbf{p_2}$ after FFF separation (left- and right-hand panels, respectively). Given are intensity-weighted radii distributions in differential and cumulative presentation of the particles in water (black solid curves) and in CCM (red dotted curves). The peak maxima are at R_h = 15 ± 1 and 23 ± 3 nm for $\mathbf{p_1}$ in water and CCM, respectively. The corresponding widths of the radii distributions for $\mathbf{p_1}$ are 5 and 14 nm, respectively. The maxima of $\mathbf{p_2}$ are R_h = 16 ± 1 and 39 ± 5 nm. The widths of the radii distributions for $\mathbf{p_2}$ are 8 and 29 nm, respectively.

(e.g., disulfide bond cleavage) after adsorption to silver nanoparticles and, hence, provide more thiol groups for a bond.[43]

To analyze the composition of the protein corona, 2-DE gels were prepared from the selected FFF fractions. Pictures of the gels are shown in Figure S3 (Supporting Information). The most abundant detected protein on $\mathbf{p_1}$ and $\mathbf{p_2}$ is BSA. This was expected because BSA is the most abundant protein in FBS and will therefore probably interact first with the particle surface.[44] Gessner et al. also presumed that hydrophilic nanoparticle surfaces mainly adsorb albumin, fibrinogen, and immunoglobulins (IgG).[45] From this list of proteins, only albumin can be detected on our particles. The complete lists of proteins for $\mathbf{p_1}$ and $\mathbf{p_2}$, respectively, are given in Tables S1 and S2 (Supporting Information). Interestingly, the long incubation time in CCM does not seem to reduce the amount of BSA in the particle corona compared to the low-abundance proteins, which may have stronger binding affinities but slower binding kinetics, as has been reported by other authors.[46] A semiquantitative analysis of protein abundance by comparing spot intensities revealed a ratio of albumin to all other proteins of 1.6 to 1 and 3.4 to 1 for $\mathbf{p_1}$ and $\mathbf{p_2}$, respectively. In the coronae of both particles, we found metal-binding proteins, which may interact with the silver ions, in addition to calcium affine proteins, e.g., S100-P, which may bind silver ions because of the similarity of the ion radii of silver (102 pm) and calcium (100 pm).[47] However, there is no preferred protein group in the corona of either particle, which makes a prediction of their physiological impacts difficult.

The hydrophilic surface of $\mathbf{p_1}$ should lead to the formation of a water shell around the particles, which would make them more inaccessible for molecules like proteins or amino acids.[48] Furthermore, several research groups have previously shown that the steric hindrance of many PEG chains, as provided here by PEG-25 glyceryl trioleate and PEG-20 sorbitan monolaurate, decreases protein adsorption. This effect is due to their brushlike structure and loop formation at the particle surface, which increases the steric hindrance of protein adsorption and also diminishes the binding of sulfur groups of the proteins to the nanoparticles' surface.[34,49] In contrast, Florin et al. showed that poly(ethylene oxide) (PEO) chains lose their adsorbed water under salty conditions,[50] and salty conditions exist in CCM. This water-releasing effect occurs mainly with shorter PEO chains, e.g., as in PEG-20 sorbitan monolaurate.[48] With more interaction between the polymer chains, gaps may occur in the brush formation on the particle surface; this results in reduced protein adsorption. PEO chains may interact with the hydrophobic α-helix and β-sheet regions of the protein. This may result in cleavage of the previously unavailable disulfide bridges and thus a strong binding to the nanoparticle surface, which makes it unavailable for other proteins in the medium. BSA, as a main component of sera, could fill this gap and would make these nanoparticles long lasting in the circulatory system.[51] Another possible explanation for the binding of only BSA could be the prolate elliptical structure of BSA. Judging from the structure of BSA, it seems reasonable that it intercalates between the chains of the stabilizers. Water exclusion between the PEO chains may lead to an inclusion of the particles, with their hydrophobic parts toward the particle surface and the hydrophilic parts interacting with the PEO chains. However, this only occurs if the entropy gain after water desorption is greater than the entropy loss due to protein freedom reduction. If the hydroxyl groups of the PEO chains are unaffected by BSA adsorption, they will collect water molecules via hydrogen bonds and thus create hydrophilicity around the particle. Moreover, this results in (a) surface inactivity of the silver core due to BSA adsorption and (b) PEO chain deformation from a more mushroomlike conformation (if the stabilizer concentration is in that range) to a brushlike conformation; this makes it even more difficult for other proteins to interact with the particles.[24]

To allow comparison to the FFF method, $\mathbf{p_1}$ was dispersed in CCM and subsequently separated from unbound proteins by centrifugation. Centrifugation was applied to compare its widespread use prior to protein-corona analysis in recent reports with our analysis combination.[7,44,52] After the centrifugation and washing steps, $\mathbf{p_1}$ exhibited more and broader protein spots (as shown in Figure S3c, Supporting Information) than the spots found in the FFF separation on the 2-DE gel. This finding indicates the presence of additional molecules and higher protein quantities than after FFF separation. This difference may lead to misinterpretation of the composition of the corona and also demonstrates the sensitivity of the FFF separation. Problems in nanoparticle characterization resulting from ultracentrifugation have been described elsewhere, and our results underline these statements.[37,53]

DOI: 10.1021/acs.langmuir.5b00687
Langmuir 2015, 31, 6842−6852

CONCLUSION

Our work demonstrates the significance of a medium-specific physicochemical nanoparticle characterization prior to in vitro experiments. The particle surface changes due to protein adsorption from the cell culture medium. Although both particle types used in our study were hydrophilic, we found differences in their protein coronae, but both have albumin as the main component. We suggest the use of asymmetric flow field-flow fractionation for gentle separation of protein-decorated particles from a protein-containing medium. Because it causes only weak shear forces, FFF is the most promising separation method for preserving the particles' complete protein corona. To our surprise, a combination of SAXS and DLS reveals that no particle aggregation was induced by the CCM for the surfactant-stabilized particles $\mathbf{p_1}$. Only a minor aggregation of 5% was determined for the PVP-stabilized particle $\mathbf{p_2}$.

Another result of our work is the medium dependency of the dissolution of the nanoparticles. Both particles revealed similar dissolution behavior in CCM after 1 day and 1 week. However, there was a concentration dependency of the release kinetics, resulting in a delayed release of ions for higher initial particle concentrations. This makes careful consideration before making a decision regarding the media of the stock solutions prior to in vitro experiments important, because Ag^+ ions are presumed to be the major cytotoxic component when cells are exposed to silver nanoparticles.

ASSOCIATED CONTENT

Supporting Information

Electron microscopy and EDX images (Figures S1 and S2), 2-DE gels images (Figure S3), and a list of identified proteins (Tables S1 and S2). The Supporting Information is available free of charge on the ACS Publications website at DOI: 10.1021/acs.langmuir.5b00687.

AUTHOR INFORMATION

Corresponding Author

*E-mail: andreas.thuenemann@bam.de. Phone: +493081041610.

Notes

The authors declare no competing financial interest.

ACKNOWLEDGMENTS

We thank Alfonso Lampen for helpful discussions; Linda Böhmert for the toxicity tests; Ilona Dörfel for scanning electron microscopy, including energy dispersive X-ray spectroscopy; and Karin Böttcher for her help during FFF fractionations. We also thank Christine Meckert and Christel Rozycki for their support during the preparation of the 1- and 2-DE gels as well as MALDI analysis. Additionally, the authors like to thank Matthias Girod and Ralph Bienert for their advice on SAXS measurements.

REFERENCES

(1) Rejeski, D. *Nanotechnology and Consumer Products*; Project on Emerging Nanotechnologies, Woodrow Wilson International Center for Scholars: Bethesda, MD, 2009; p 12.

(2) Rogers, K. R.; Bradham, K.; Tolaymat, T.; Thomas, D. J.; Hartmann, T.; Ma, L. Z.; Williams, A. Alterations in physical state of silver nanoparticles exposed to synthetic human stomach fluid. *Sci. Total Environ.* **2012**, *420*, 334−339.

(3) Potočnik, J. *Commission Recommendation of 18 October 2011 on the Definition of Nanomaterial Text with EEA Relevance*; European Commision: Brussels, 2011; p 38−40.

(4) Karmali, P. P.; Simberg, D.Interactions of nanoparticles with plasma proteins: Implication on clearance and toxicity of drug delivery systems *Expert Opin. Drug Delivery 8*, 343−357.

(5) Nel, A. E.; Madler, L.; Velegol, D.; Xia, T.; Hoek, E. M. V.; Somasundaran, P.; Klaessig, F.; Castranova, V.; Thompson, M. Understanding biophysicochemical interactions at the nano−bio interface. *Nat. Mater.* **2009**, *8*, 543−557.

(6) Maiorano, G.; Sabella, S.; Sorce, B.; Brunetti, V.; Malvindi, M. A.; Cingolani, R.; Pompa, P. P. Effects of cell culture media on the dynamic formation of protein−nanoparticle complexes and influence on the cellular response. *ACS Nano* **2010**, *4*, 7481−7491.

(7) Casals, E.; Pfaller, T.; Duschl, A.; Oostingh, G. J.; Puntes, V. Time evolution of the nanoparticle protein corona. *ACS Nano* **2010**, *4*, 3623−3632.

(8) Milani, S.; Bombelli, F. B.; Pitek, A. S.; Dawson, K. A.; Radler, J. Reversible versus irreversible binding of transferrin to polystyrene nanoparticles: Soft and hard corona. *ACS Nano* **2012**, *6*, 2532−2541.

(9) Beer, C.; Foldbjerg, R.; Hayashi, Y.; Sutherland, D. S.; Autrup, H. Toxicity of silver nanoparticles—Nanoparticle or silver ion? *Toxicol. Lett.* **2011**, *208*, 286−292.

(10) Andrlik, I. Einfluss der nichtionischen Tenside Tween 20, Tween 80 und Pluronic F-68 auf die Interaktion von Nanopartikeln mit Caco-2 Einzelzellen. Diploma Thesis; University of Wien, Vienna, Austria, 2008.

(11) Baier, G.; Costa, C.; Zeller, A.; Baumann, D.; Sayer, C.; Araujo, P. H. H.; Mailander, V.; Musyanovych, A.; Landfester, K.BSA adsorption on differently charged polystyrene nanoparticles using isothermal titration calorimetry and the influence on cellular uptake *Macromol. Biosci. 11*, 628−638.

(12) Wang, F. J.; Yu, L.; Monopoli, M. P.; Sandin, P.; Mahon, E.; Salvati, A.; Dawson, K. A. The biomolecular corona is retained during nanoparticle uptake and protects the cells from the damage induced by cationic nanoparticles until degraded in the lysosomes. *Nanomedicine (N. Y., NY, U. S.)* **2013**, *9*, 1159−1168.

(13) Lesniak, A.; Fenaroli, F.; Monopoli, M. R.; Aberg, C.; Dawson, K. A.; Salvati, A. Effects of the presence or absence of a protein corona on silica nanoparticle uptake and impact on cells. *ACS Nano* **2012**, *6*, 5845−5857.

(14) Kim, J. A.; Salvati, A.; Aberg, C.; Dawson, K. A. Suppression of nanoparticle cytotoxicity approaching in vivo serum concentrations: Limitations of in vitro testing for nanosafety. *Nanoscale* **2014**, *6*, 14180−14184.

(15) Ahamed, M.; AlSalhi, M. S.; Siddiqui, M. K. J. Silver nanoparticle applications and human health. *Clin. Chim. Acta* **2010**, *411*, 1841−1848.

(16) Gopinath, P.; Gogoi, S. K.; Sanpui, P.; Paul, A.; Chattopadhyay, A.; Ghosh, S. S.Signaling gene cascade in silver nanoparticle induced apoptosis *Colloids Surf. B. 77*, 240−245.

(17) Hsin, Y. H.; Chena, C. F.; Huang, S.; Shih, T. S.; Lai, P. S.; Chueh, P. J. The apoptotic effect of nanosilver is mediated by a ROS- and JNK-dependent mechanism involving the mitochondrial pathway in NIH3T3 cells. *Toxicol. Lett.* **2008**, *179*, 130−139.

(18) Hussain, S. M.; Hess, K. L.; Gearhart, J. M.; Geiss, K. T.; Schlager, J. J. In vitro toxicity of nanoparticles in BRL 3A rat liver cells. *Toxicol. In Vitro* **2005**, *19*, 975−983.

(19) Bouwmeester, H.; Dekkers, S.; Noordam, M. Y.; Hagens, W. I.; Bulder, A. S.; de Heer, C.; ten Voorde, S.; Wijnhoven, S. W. P.; Marvin, H. J. P.; Sips, A. Review of health safety aspects of nanotechnologies in food production. *Regul. Toxicol. Pharmacol.* **2009**, *53*, 52−62.

(20) Foldbjerg, R.; Olesen, P.; Hougaard, M.; Dang, D. A.; Hoffmann, H. J.; Autrup, H. PVP-coated silver nanoparticles and silver ions induce reactive oxygen species, apoptosis and necrosis in THP-1 monocytes. *Toxicol. Lett.* **2009**, *190*, 156−162.

(21) Hassellov, M.; Readman, J. W.; Ranville, J. F.; Tiede, K. Nanoparticle analysis and characterization methodologies in environ-

DOI: 10.1021/acs.langmuir.5b00687
Langmuir 2015, 31, 6842−6852

mental risk assessment of engineered nanoparticles. *Ecotoxicology* **2008**, *17*, 344−361.
(22) Bohmert, L.; Girod, M.; Hansen, U.; Maul, R.; Knappe, P.; Niemann, B.; Weidner, S. M.; Thunemann, A. F.; Lampen, A. Analytically monitored digestion of silver nanoparticles and their toxicity on human intestinal cells. *Nanotoxicology* **2014**, *8*, 631−42.
(23) Thunemann, A. F.; Knappe, P.; Bienert, R.; Weidner, S. Online coupling of field-flow fractionation with SAXS and DLS for polymer analysis. *Anal. Methods* **2009**, *1*, 177−182.
(24) Norde, W.; Gage, D. Interaction of bovine serum albumin and human blood plasma with PEO-tethered surfaces: Influence of PEO chain length, grafting density, and temperature. *Langmuir* **2004**, *20*, 4162−4167.
(25) Torchilin, V. P.; Trubetskoy, V. S. Which polymers can make nanoparticulate drug carriers long-circulating? *Adv. Drug Delivery Rev.* **1995**, *16*, 141−155.
(26) Treuel, L.; Malissek, M.; Grass, S.; Diendorf, J.; Mahl, D.; Meyer-Zaika, W.; Epple, M.Quantifying the influence of polymer coatings on the serum albumin corona formation around silver and gold nanoparticles *J. Nanopart. Res.* **2012**, *14*.
(27) Prestel, H.; Niessner, R.; Panne, U. Increasing the sensitivity of asymmetrical flow field-flow fractionation: Slot outlet technique. *Anal. Chem.* **2006**, *78*, 6664−6669.
(28) Pauw, B. R. Everything SAXS: Small-angle scattering pattern collection and correction. *J. Phys.: Condens. Matter* **2013**, *25*, 383201.
(29) Breßler, I.; Pauw, B. R.; Thünemann, A. F. McSAS Software for the retrieval of model parameter distributions from scattering patterns. *J. Appl. Cryst.* **2015**, *48*, 962−969.
(30) Bolea, E.; Jimenez-Lamana, J.; Laborda, F.; Abad-Alvaro, I.; Blade, C.; Arola, L.; Castillo, J. R. Detection and characterization of silver nanoparticles and dissolved species of silver in culture medium and cells by AsFlFFF−UV−Vis−ICPMS: Application to nanotoxicity tests. *Analyst* **2014**, *139*, 914−922.
(31) Huynh, K. A.; Chen, K. L. Aggregation kinetics of citrate and polyvinylpyrrolidone coated silver nanoparticles in monovalent and divalent electrolyte solutions. *Environ. Sci. Technol.* **2011**, *45*, 5564−5571.
(32) Zook, J. M.; Long, S. E.; Cleveland, D.; Geronimo, C. L. A.; MacCuspie, R. I. Measuring silver nanoparticle dissolution in complex biological and environmental matrices using UV−visible absorbance. *Anal. Bioanal. Chem.* **2011**, *401*, 1993−2002.
(33) Balmer, J. A.; Mykhaylyk, O. O.; Schmid, A.; Armes, S. P.; Fairclough, J. P. A.; Ryan, A. J. Characterization of polymer−silica nanocomposite particles with core−shell morphologies using Monte Carlo simulations and small angle X-ray scattering. *Langmuir* **2011**, *27*, 8075−8089.
(34) Vonarbourg, A.; Passirani, C.; Saulnier, P.; Benoit, J. P. Parameters influencing the stealthiness of colloidal drug delivery systems. *Biomaterials* **2006**, *27*, 4356−4373.
(35) Kittler, S.; Greulich, C.; Diendorf, J.; Koller, M.; Epple, M. Toxicity of silver nanoparticles increases during storage because of slow dissolution under release of silver ions. *Chem. Mater.* **2010**, *22*, 4548−4554.
(36) Bohmert, L.; Hansen, U.; Girod, M.; Knappe, P.; Niemann, B.; Thunemann, A.; Lampen, A. Cytotoxicity of AgPure silver nanoparticles in the human intestinal cell line Caco-2. *Toxicol. Lett.* **2011**, *205*, S280−S280.
(37) Bouwmeester, H.; Poortman, J.; Peters, R. J.; Wijma, E.; Kramer, E.; Makama, S.; Puspitaninganindita, K.; Marvin, H. J. P.; Peijnenburg, A. A. C. M.; Hendriksen, P. J. M.Characterization of translocation of silver nanoparticles and effects on whole-genome gene expression using an in vitro intestinal epithelium coculture model *ACS Nano 5*, 4091−4103.
(38) Smith, F. C. The Ultra-Violet Absorption Spectra of Certain Aromatic Amino-Acids, and of the Serum Proteins. *Proc. R. Soc. London., Ser. B* **1929**, *104*, 198−205.
(39) Giddings, J. C. Field-flow fractionation—Analysis of macromolecular, colloidal, and particulate materials. *Science* **1993**, *260*, 1456−1465.
(40) Ferrer, M. L.; Duchowicz, R.; Carrasco, B.; de la Torre, J. G.; Acuna, A. U. The conformation of serum albumin in solution: A combined phosphorescence depolarization−hydrodynamic modeling study. *Biophys. J.* **2001**, *80*, 2422−2430.
(41) Gondikas, A. P.; Morris, A.; Reinsch, B. C.; Marinakos, S. M.; Lowry, G. V.; Hsu-Kim, H.Cysteine-induced modifications of zero-valent silver nanomaterials: Implications for particle surface chemistry, aggregation, dissolution, and silver speciation *Environ. Sci. Technol. 46*, 7037−45.
(42) Wigginton, N. S.; Titta, A. d.; Piccapietra, F.; Dobias, J.; Nesatyy, V. J.; Suter, M. J. F.; Bernier-Latmani, R. Binding of silver nanoparticles to bacterial proteins depends on surface modifications and inhibits enzymatic activity. *Environ. Sci. Technol.* **2010**, *44*, 2163−2168.
(43) Han, J.; Liu, Y.; Guo, R. Reactive template method to synthesize gold nanoparticles with controllable size and morphology supported on shells of polymer hollow microspheres and their application for aerobic alcohol oxidation in water. *Adv. Funct. Mater.* **2009**, *19*, 1112−1117.
(44) Cedervall, T.; Lynch, I.; Foy, M.; Berggad, T.; Donnelly, S. C.; Cagney, G.; Linse, S.; Dawson, K. A. Detailed identification of plasma proteins adsorbed on copolymer nanoparticles. *Angew. Chem., Int. Ed.* **2007**, *46*, 5754−5756.
(45) Gessner, A.; Waicz, R.; Lieske, A.; Paulke, B. R.; Mader, K.; Muller, R. H. Nanoparticles with decreasing surface hydrophobicities: Influence on plasma protein adsorption. *Int. J. Pharm.* **2000**, *196*, 245−249.
(46) Cedervall, T.; Lynch, I.; Lindman, S.; Berggard, T.; Thulin, E.; Nilsson, H.; Dawson, K. A.; Linse, S. Understanding the nanoparticle−protein corona using methods to quantify exchange rates and affinities of proteins for nanoparticles. *Proc. Natl. Acad. Sci. U. S. A.* **2007**, *104*, 2050−2055.
(47) Shannon, R. Revised effective ionic radii and systematic studies of interatomic distances in halides and chalcogenides. *Acta Crystallogr., Sect. A* **1976**, *32*, 751−767.
(48) Stolnik, S.; Illum, L.; Davis, S. S. Long circulating microparticulate drug carriers. *Adv. Drug Delivery Rev.* **1995**, *16*, 195−214.
(49) Gref, R.; Domb, A.; Quellec, P.; Blunk, T.; Muller, R. H.; Verbavatz, J. M.; Langer, R. The controlled intravenous delivery of drugs using PEG-coated sterically stabilized nanospheres. *Adv. Drug Delivery Rev.* **1995**, *16*, 215−233.
(50) Florin, E.; Kjellander, R.; Eriksson, J. C. Salt effects on the cloud point of the poly(ethylene oxide) + water system. *J. Chem. Soc., Faraday Trans. 1* **1984**, *80*, 2889−2910.
(51) Gradishar, W. J.; Tjulandin, S.; Davidson, N.; Shaw, H.; Desai, N.; Bhar, P.; Hawkins, M.; O'Shaughnessy, J. Phase III trial of nanoparticle albumin-bound paclitaxel compared with polyethylated castor oil based paclitaxel in women with breast cancer. *J. Clin. Oncol.* **2005**, *23*, 7794−7803.
(52) Dell'Orco, D.; Lundqvist, M.; Oslakovic, C.; Cedervall, T.; Linse, S.Modeling the time evolution of the nanoparticle−protein corona in a body fluid *PLoS One 5*, 8.
(53) Aggarwal, P.; Hall, J. B.; McLeland, C. B.; Dobrovolskaia, M. A.; McNeil, S. E. Nanoparticle interaction with plasma proteins as it relates to particle biodistribution, biocompatibility and therapeutic efficacy. *Adv. Drug Delivery Rev.* **2009**, *61*, 428−437.

DOI: 10.1021/acs.langmuir.5b00687
Langmuir 2015, 31, 6842−6852